Advanced VCSEL Technology: Self-Heating and Intrinsic Modulation Response

Dennis G. Deppe, *Fellow, IEEE*, Mingxin Li, Xu Yang, and Mina Bayat

(Invited Paper)

***Abstract*— Experimental data and modeling results are presented for a new type of vertical-cavity surface-emitting laser (VCSEL) that solves numerous problems with oxide VCSELs. In addition, the new oxide-free VCSEL can be scaled to small size. Modeling shows that this small size can dramatically increase the speed of the laser through control of self-heating. Modeling compared with both the oxide and the new oxide-free VCSEL predict intrinsic modulation speed for room temperature approaching 80 GHz, indicating the potential for > 100-Gb/s data speed from directly modulated VCSELs. The modeling is one of if not the first to include self-heating and spectral detuning between the gain and the cavity resonance that results from self-heating. The modeling results accurately accounts for the saturation in modulation speed in very high-speed oxide VCSELs operating at high temperature and accounts for the temperature of differential gain and photon density in limiting speed. Saturation of the photon density is found to limit the ultimate intrinsic speed. Differential gain decreases with increasing temperature but with sufficiently weak temperature dependence that it is not found to limit the VCSEL speed.**

***Index Terms*— Vertical cavity surface emitting lasers, oxide aperture, high speed modulation, laser physics, semiconductor devices, optical data transmission.**

I. Introduction

VERTICAL-CAVITY surface-emitting lasers (VCSELs) [1] have come to dominate commercial laser technologies for low power laser diodes. Work on epitaxial mirrors in the late 1980's led to numerous performance break-throughs by providing mirror reflectivities for upper and lower mirrors that can be matched to high performance quantum well (QW) gain material [2]–[13].

At the same time the work on epitaxial mirrors provided a more subtle but powerful improvement in the VCSEL through improved thermal performance [2]–[13]. The all-semiconductor cavity based on the epitaxial mirrors can efficiently conduct heat from the strongly pumped laser active volume, and in a laser cavity much smaller than possible before with commercial edge-emitting laser diodes.

This change made it possible to obtain much higher current density, and therefore higher photon density, and higher stimulated emission rate than other laser diodes. Continually reducing the laser active volume and relying on relatively high efficiency VCSEL designs have produced ever-increasing laser diode speed. VCSELs now reign supreme in laboratory demonstrations of direct modulation data speed due largely to their combined small volume, matched cavity and gain region, and high internal heat flow through high quality epitaxial mirrors [15]–[23].

For the last twenty years there have also been research efforts to develop alternative routes to low power laser diodes using a variety of other cavity types [25]–[30]. These have included photonic crystal cavities, metal cavities, posts or nanorods, and microdisks. Despite extensive research, to date these have failed to produce viable alternatives to VCSELs. A photonic crystal cavity, for example, has relatively poor optical extraction efficiency when compared to a VCSEL, and suffers from high electrical and thermal resistance inherent to its cavity. Metal cavities high internal absorption and provide inadequate reflectivity to match high quality laser diode gain material. They suffer poor thermal performance and poor optical extraction efficiency caused by metal absorption. If the metal cavities are made very small they create a second loss mechanism due to nonradiative energy transfer directly between the active emitters and metal. This interesting physics has been studied in some detail, and the metal interaction with a radiating dipole is a killer of efficiency for both lasers and spontaneous emitters [31], [32].

Small vertical cavity spontaneous emitters and VCSELs that use both the epitaxial mirrors and additional transverse confinement structures have also been researched. The most successful in the commercial sector has been the oxide-apertured VCSELs developed at the University of Texas by one of the authors (DGD) and his collaborators at that time [33]. These studies showed that oxide VCSELs could be made with much smaller active volume while retaining higher efficiency than the proton implanted VCSELs. The oxide-apertured VCSEL has set repeated records in direct modulation speed and efficiency needed for high speed, high efficiency optical interconnects and sensors [34]–[36]. The oxide VCSEL is responsible for all current laser diode speed records [15]–[24].

The oxide VCSEL has ushered in new markets for these small laser diodes that include data centers, printers,

Manuscript received January 23, 2018; revised March 28, 2018; accepted April 3, 2018. Date of publication April 13, 2018; date of current version April 20, 2018. This work was supported in part by the Army Research Office under Grant W911NF1510579 and in part by a MURI grant from the Air Force Office of Sponsored Projects administered by the University of Texas at Austin under Grant FA95501710071. *(Corresponding author: Mina Bayat.)*

D. G. Deppe and M. Bayat are with the College of Optics and Photonics, University of Central Florida, Orlando, FL 32186 USA (e-mail: ddeppe@creol.ucf.edu; minabayat@knights.ucf.edu).

M. Li was with the College of Optics and Photonics, University of Central Florida, Orlando, FL 32186 USA. He is now with Lumentum, Milpitas, CA 95035 USA.

X. Yang was with the College of Optics and Photonics, University of Central Florida, Orlando, FL 32186 USA. He is now with Accelink Company, Wuhan 430205, China.

Color versions of one or more of the figures in this paper are available online at http://ieeexplore.ieee.org.

Digital Object Identifier 10.1109/JQE.2018.2826718

and laser mice. More recently cellphone sensors capable of 3-dimensional sensing, using VCSELs have become available. And the oxide VCSEL continues to be the record holder in high-speed direct modulation and efficiency for commercial optical interconnects. Oxide VCSEL optical interconnects deliver both lower bit energy and lower cost than alternative optical modulator-based technologies. And compared to directly modulated edge-emitting laser diodes, the VCSEL wins out in cost, speed, and efficiency because of its small active volume and surface emitting arrays.

The keys to the successes of the VCSEL and its small cavity have been its epitaxial mirrors that provide high heat flow, high reflectivity, and low optical loss, along with its efficient operation. Although oxide VCSELs now dominate commercial low power laser diode markets, the reliance on the oxide aperture does not yet fully extract the benefits of possible with small laser diodes fabricated fully out of epitaxial materials. The success of the VCSEL has also apparently obscured the limitations of the oxide aperture. The oxide VCSEL suffers from poor heat flow in key regions of the laser cavity that produce self-heating and spectral detuning. The epitaxial mirrors of the oxide VCSEL also suffer from the material choices needed for the oxidation step to create the aperture. The oxide aperture causes further problems with cavity volume reduction tied to mechanical stress of the oxide and manufacturing yield limited by variations in the aperture size. All these suggest that VCSELs still do not operate close to their ideal laser diode performance. We also show below that further size scaling, which is fully possible in a VCSEL cavity, can potentially bring important advances in speed and efficiency for high speed optical interconnects.

In the analysis presented here the physics controlling the temperature dependence of the differential gain and photon saturation in the cavity under high drive levels are studied. We use measured results from oxide and a new type of oxide-free VCSEL to compare intrinsic modulation speed with with this thermal limits. One problem that has limited the development of small cavity laser diodes has been the lack of a model that accurately accounts for and can analyze self-heating. We present this model below to gain predictive ability of how improved VCSEL designs that eliminate oxide apertures can increase modulation speed.

Unlike detectors or many optical modulators, laser diodes generally operate while dissipating a high thermal power density in their active volume. Self-heating becomes an important predictor of laser diode performance, especially in high-speed modulation and small cavity laser diodes. An important aspect of the model is the inclusion of spectral detuning due to the small cavity and high drive levels. The ability to include spectral detuning allows analysis of the high-speed laser diode modulation, at least for VCSELs, in more detail than, to our knowledge, has been previously possible. The model is used to analyze the intrinsic modulation speed to determine the roles of internal self-heating and differential gain of the active region.

Although many researchers have proposed that speed limits are due to the temperature dependence of the differential gain, we do not directly find this in our analysis. Instead the results show that intrinsic speed of the laser diode is limited by saturation of the internal photon density due to thermally driven spectral detuning between the cavity and gain region. Because this detuning is due to internal self-heating, reducing the internal operating temperature of the laser becomes a key technical challenge to address to produce a next generation in high speed VCSELs. Reducing the active volume and decreasing internal laser diode temperature are further shown to be interrelated and important. The modeling results predict that with control of internal self-heating, high efficiency, and cavity scaling, optimized VCSELs should be capable of reaching direct modulation speeds needed for $>$ 100 Gb/s data rate.

In this paper we also present record setting performance levels measured in a new oxide-free VCSEL technology. The oxide-free aperture technology is fully epitaxial and relies on a shallow mesa. Current confinement uses a proprietary structure that is part of the epitaxy. The resulting oxide-free VCSEL produces very high efficiency for small cavity laser diodes [38]. This could enable reliable manufacturing of laser diodes based on the oxide-free VCSELs that have small cavity volume. Cavity volume could reduce by more than two orders of magnitude smaller than the smallest commercial laser diode now available. The VCSEL geometry appears to produce the optimum combination of low optical loss, low electrical resistance, and low thermal resistance to enable this decrease in laser size. This combination promises high efficiency nanoscale laser diodes in the form of nano-VCSELs that can produce higher speed, greater efficiency for low power applications including high speed optical interconnects and sensors.

II. Model

To model the temperature dependence of the small cavity lasers, the laser rate equations are written to include the temperature dependence of electron-hole distributions in their respective bands, and the temperature dependence of spectral detuning between the cavity and gain material. The rate equation can be given in terms of photon numbers, electron numbers and their temperature dependence as

$$\frac{dn_m(t,T_J)}{dt} = -\frac{\omega_{c,m}}{Q_m}(T_J)n_m(t,T_J)+g_{st,m}(N_e,T_J)n_m(t,T_J) + g_{sp,m}(N_e,T_J) \quad (1)$$

$$\frac{dN_e(t,T_J)}{dt} = \frac{I(t)}{q} - \sum_m [g_{st,m}(N_e,T_J)n_m(t,T_J) + g_{sp,m}(N_e,T_J)] \quad (2)$$

where n_{m} is photon number of the m-th mode in the cavity, N_{e} is the number of electrons in the active region, $\omega_{\mathrm{c,m}}$ is the lasing frequency in the cavity, Q_{m} is the quality factor, T_{J} is junction temperature, I is the bias current, q is the charge of an electron, and $g_{\mathrm{sp,m}}$ is the spontaneous emission coefficient. Intrinsic modulation speed as set by the laser gain and cavity depends on the differential gain with respect to the electron number or concentration, $\frac{dg_{st,m}}{dN_{\mathrm{e}}}$, the cavity loss rate $\frac{\omega_{\mathrm{c,m}}}{Q_{\mathrm{m}}}$, and the photon number n_{m}. The cavity loss rate in small cavity laser diodes will in general include nonneglible free carrier absorption. This free carrier absorption is one of

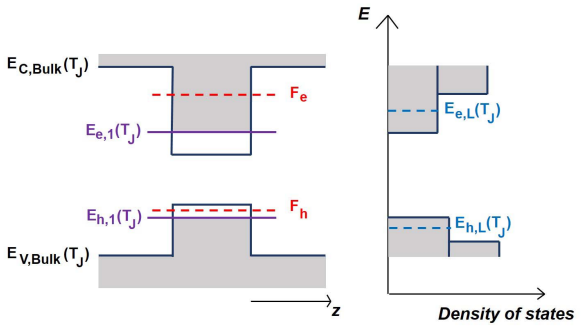

Fig. 1. The electronic structure and density of states for a 2D quantum well.

the main heating mechanisms of the laser cavity. Here we include the effect on self-heating through the efficiency loss of the laser but assume otherwise the cavity quality factor remains unchanged. This is equivalent to assuming that the free carrier absorption coefficients are temperature independent.

The temperature dependent gain and differential gain can be found from assuming quasi-Fermi distributions for electrons and holes in their respective energy levels and bands. Fig. 1 shows the band structure and electronic densities of states used to calculate both these parameters. Momentum and energy conservation are assumed to produce the typically assumed selection rules for optical transitions between electron and hole states. The small cavities can be assumed to be single mode with respect to the quantum well's confinement regions. Here we consider planar quantum wells as opposed to quantum wires or quantum dots, since the optical gain can be higher using planar quantum wells. Non-ideal fill factors reduce the gain of either quantum wires or quantum dots and offset and we find these to offset advantages that may otherwise come from improved spectral overlap between the optical gain and cavity.

Given the above assumptions, quasi-Fermi energies can be used with the electronic density of states to analyze the temperature dependent carrier densities under various current drive and modulation conditions. Therefore, quasi-Fermi energies give both the voltage drive over the laser gain region and the carrier populations in the planar quantum wells. The gain coefficient for stimulated emission can be written in terms of the specific electron and hole lasing transitions of Fig. 1 and the respective electron and hole quasi-Fermi energies, and is given by

$$g_{st,m} = \Gamma_{QW} N_{QW} g_{QW,m}\left[\frac{1}{\exp\left(\frac{E_{e,L}(T_J)-F_e}{k_B T_J}\right)+1} - \frac{1}{\exp\left(\frac{E_{h,L}(T_J)-F_h}{k_B T_J}\right)+1}\right] \quad (3)$$

N_{QW} in Eq. (3) is the number of quantum wells in the active region, Γ_{QW} is the normalized confinement factor, F_e and F_h are the electron and hole quasi-Fermi levels, $E_{e,L}$ and $E_{h,L}$ are electron and hole energy levels that are participating in lasing, and k_B is the Boltzmann constant. Γ_{QW} is the 3-dimensional confinement factor where we have assumed the transverse confinement is unity. $g_{QW,m}$ includes the dipole strength of the planar quantum wells, and along with constant factors is given by

$$g_{QW} = \frac{2\pi c^3 m_r}{\tau_{sp} L_z \hbar n_r^3 \omega_c^2} \quad (4)$$

where m_r is the reduced effective mass of an electron and hole pair, n_r is refractive index in the active region, and L_z is effective cavity length in z direction (direction of the quantum well thickness). τ_{sp} is the spontaneous lifetime due to the semiconductor dipole transition, assuming a filled electron state and empty hole state. In Eq. (4) normalized field strength is used that accounts for the actual confined laser field intensity in the semiconductor cavity.

Fig. 1 shows the electronic structure and density of states in a 2D quantum well. The electron and hole numbers in the quantum well gain material are calculated using the electronic density of states that results from the quantum well gain region, and the quasi-Fermi energy positions as given in Eq. (5) and Eq. (6). We assume that the quantum wells are sufficiently thin that only one electron state is confined in the well (Fig. 1 shows a more general case with two) and two holes. More quantized states can be included following the similar procedure. Bulk states are included in Eqs. (5) and (6) using the Boltzmann approximation for Fermi occupation of charge carriers.

Capturing the temperature dependence of cavity detuning from the spectral gain is achieved by allowing both electronic energy level positions and the cavity resonance to have temperature dependence. Therefore though not explicitly shown in Eq. (5) and Eq. (6), the electronic energy levels $E_{e,L}(T_J)$ and $E_{h,L}(T_J)$ shift with junction temperature in the simulations given below. Also shifting with temperature are the electronic levels that set the densities of states in different energy regions.

$$\begin{aligned} N_e &= N_{e,QW} + N_{e,Bulk} \\ N_e &= \frac{A_{QW} k_B T_J}{\pi \hbar^2}\{N_{QW} m_e \ln\left[\exp\left(-\frac{E_{e,1}(T_J)-F_e}{k_B T_J}\right)1 \right. \\ &\quad \left. + \exp\left(-\frac{E_{C,Bulk}(T_J)-F_e}{k_B T_J}\right)+1\right] \\ &\quad + \left(N_{QW} L_{z,QW} m_e^{\frac{3}{2}} + L_{z,Bulk} m_{e,Bulk}^{\frac{3}{2}}\right)\left(\frac{k_B T_J}{2\pi\hbar^2}\right)^{\frac{1}{2}} \\ &\quad \times \exp\left(-\frac{E_{C,Bulk}(T_J)-F_e}{k_B T_J}\right)\} \end{aligned} \quad (5)$$

$$\begin{aligned} N_h &= N_{h,QW} + N_{h,Bulk} \\ N_h &= \frac{A_{QW} k_B T_J}{\pi \hbar^2}\{N_{QW} m_{h,m} \ln\left[\frac{\exp\left(-\frac{E_{h,m}(T_J)-F_h}{k_B T_J}\right)+1}{\exp\left(-\frac{E_{V,Bulk}(T_J)-F_h}{k_B T_J}\right)+1}\right] \\ &\quad + \left(N_{QW} L_{z,QW} m_h^{\frac{3}{2}} + L_{z,Bulk} m_{h,Bulk}^{\frac{3}{2}}\right)\left(\frac{k_B T_J}{2\pi\hbar^2}\right)^{\frac{1}{2}} \\ &\quad \exp\left(-\frac{E_{V,Bulk}(T_J)-F_h}{k_B T_J}\right)\} \end{aligned} \quad (6)$$

where $E_{e,1}(T_J($ and $E_{h,m}(T_J)$ (m = 1, 2) are the sub band energy levels of electrons and holes. $E_{C,Bulk}(T_J($ and $E_{V,Bulk}$ are the energy levels of the conduction and valance band edge of the bulk material.m_e and $m_{h,m}$ are the effective masses of electrons and holes in the quantum wells, $m_{e,Bulk}$ and $m_{h,Bulk}$

are the effective masses of electrons and holes of the bulk material. A_{QW} is the area of the quantum wells in x-y plane perpendicular to the direction of quantum well thickness (z) and L_z is the thickness in z direction. We assume charge neutrality in the quantum well gain region that includes the thermal populations in the bulk states of the gain region,

$$N_e(t, T_J) = N_h(t, T_J) \tag{7}$$

where N_h is the number of holes in the active region.

The expression for the intrinsic modulation response that is derived from semiconductor rate Eqs. (1) and (2) is given by

$$H_I(\omega) = \frac{\frac{\omega_c}{Q}(T)\Delta n(\omega, T)}{\frac{\Delta I(\omega)}{q}} \approx \frac{\frac{\omega_c}{Q}(T)G_{Diff}(T)n_0(T)}{-\omega^2 - i\omega G_{Diff}(T)n_0(T) + \frac{\omega_c}{Q}(T)G_{Diff}(T)n_0(T)} \tag{8}$$

where $n_0(T_J)$ is the number of photons in QW resulted from solving the rate equations in steady state. G_{Diff} is differential gain and is a function of junction temperature, electronic structure and quasi-Fermi energies which itself has a relation with electron numbers (N_e) and it can be found by solving the rate equations in steady state. It can be shown that G_{Diff} is (9), as shown in the bottom of the next page. The above expression for the differential gain coefficient relates the differential gain to the positions of the quasi-Fermi levels within the electronic structure. As the internal temperature T_J increases with increasing bias current due to self-heating, the differential gain decreases due to both the increasing thermal distribution of electrons and holes in the energy levels and the increasing spectral detuning. Once a given drive level is exceeded the photon density also saturates, leaving an open question on which is the more important limiting factor.

Several experimental reports of high-speed oxide VCSELs now include sufficient details of their internal design that the published experimental device results can be compared with the modeling. By including reported thermal resistance and cavity design parameters we are able to account for power dissipation in the VCSEL and its influence on self-heating and spectral detuning.

Fig. 2 shows comparisons of the calculations with results obtained for a high speed 7 μm diameter oxide VCSEL measurements published by Chalmers University [20]. The highest speed of the oxide VCSEL measured by Chalmers was reported to be 27 GHz for the room temperature operation (RT) at ~14 mA bias current. This measurement includes both intrinsic bandwidth of the VCSEL and the electrical parasitics. The model predicts that the intrinsic speed at that bias current is closer to 29 GHz. Therefore except for the highest room temperature speed of 27 GHz, the other measured speeds for lower bias current and 85°C operation reflect the limitation due to intrinsic speed. Therefore, the model including spectral detuning accurately captures the thermal saturation of the modulation speed.

Below we show it is the saturating photon density that limits the intrinsic speed. We also note that intrinsic speed also

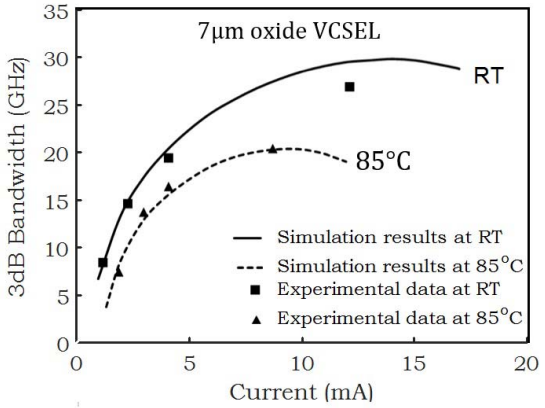

Fig. 2. Comparison of 3dB bandwidth between simulation results and experimental data of a 7 μm oxide VCSEL. Experimental data is taken from [20].

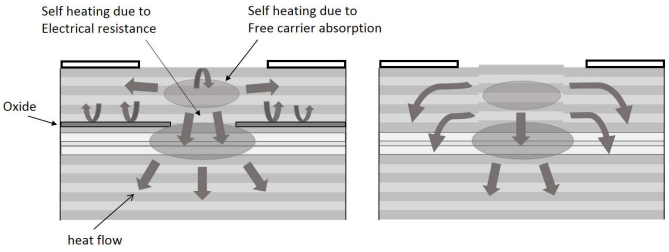

Fig. 3. (Left) Heat flow in oxide VCSELs. (Right) Heat flow in oxide-free VCSELs.

limits the oxide VCSELs overall speed from Fig. 2, since the laser must operate at 85°C. At this operating temperature the intrinsic speed limits the overall speed, and electrical parasitics have lesser impact.

III. Oxide-Free VCSEL

Fig. 3 shows schematic cross sections comparing the heat flow in either oxide or oxide-free VCSELs. The heat flow caused by the oxide aperture that leads to the higher thermal resistance is part of the reason for the oxide VCSEL having a thermal resistance much higher than that possible based on its ideal materials. The selective oxidation was developed at the University of Illinois by Dallesasse *et al.* [38], [39] several years prior to the demonstration of the oxide VCSEL [33] and has also been used in edge-emitters by Holonyak's group [39]. In a VCSEL the oxide aperture requires that AlGaAs with ~90% Al composition be used in the upper mirror stack for layers intended for only partial oxidation. The one or more AlGaAs layers used to form the oxide aperture are typically ~98%. However, neither AlGaAs compositions are ideal mirror materials, since the 90% AlGaAs higher refractive index and much lower thermal conductivity than AlAs [40].

The oxide aperture directly blocks the heat flow in the VCSEL as shown in Fig. 3, forcing the heat back up into the upper p-mirror. Because a reactively ion etched post must also be formed to perform the selective oxidation and form the oxide aperture, the resulting oxidation post also blocks lateral heat flow away from the VCSEL's active volume. The

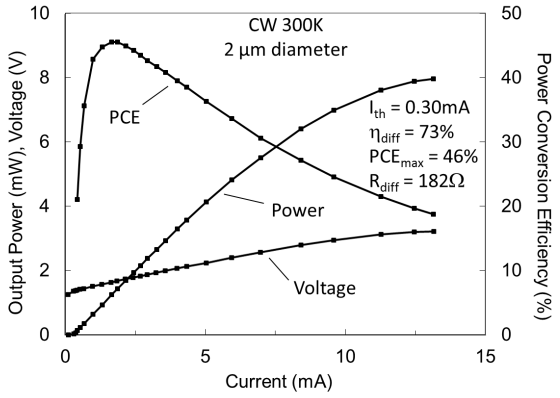

Fig. 4. Voltage, power and PCE vs. current of a 2 μm diameter oxide-free, lithographic VCSEL under CW operation at room temperature.

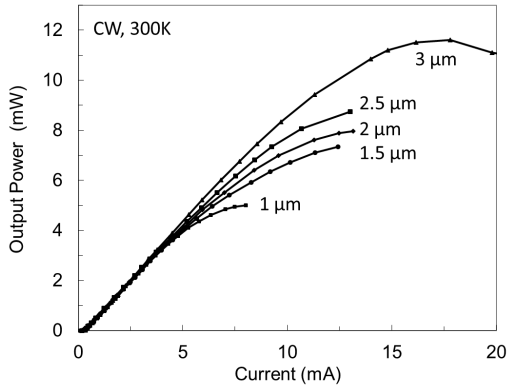

Fig. 5. L-I curves for the 1, 1.5, 2, 2.5, 3 μm diameter oxide-free VCSEL measured CW at room temperature.

result is that heat is forced to flow through the aperture. These differences result in the oxide VCSEL having three to four times the thermal resistance of the oxide-free VCSEL [40].

The oxide-free VCSEL includes internal optical and electrical confinement comparable to and even exceeding the oxide aperture, and uses a proprietary internal confinement structure that is fully epitaxial [37], [40]–[43]. This fully epitaxial aperture dramatically increases lateral heat flow and reduces the VCSELs operating junction temperature for a given current density. The reduction in thermal resistance and junction temperature in the oxide-free VCSEL when compared with the oxide VCSEL is quite dramatic and has been reported elsewhere [40]. The interest here is the potential to use the new structure to reach much higher modulation speeds than possible today using other laser diodes.

Fig. 4 shows light vs. current and voltage vs. current (LIV) curves for a 2 μm oxide-free VCSEL. The impact of the improved cooling can be seen from the high power density that can be obtained under continuous-wave (CW) operation at room temperature. As shown in Fig. 4, the threshold current of the device is 0.30 mA, maximum output power is 7.97 mW, maximum differential quantum efficiency is 73%, and its maximum power conversion efficiency is 46%. We believe these are each record values for a laser diode with this small of combined gain and cavity volume.

Fig. 5 shows LI measurements for a variety of sizes ranging from 1 μm to 3 μm in diameter. The lasing characteristics, including threshold currents, maximum power, differential quantum efficiency (D.Q.E.), power conversion efficiency (P.C.E.) and voltage at 10 kA/cm^2, are listed in Table I.

In Table I, the threshold of the smallest VCSEL increases due to a number of loss mechanisms. These include both electronic loss and optical loss due to aperture perimeter effects.

We have also studied the internal temperature of the oxide-free and oxide VCSELs experimentally. Fig. 6 shows measurements for a 3 μm diameter oxide-free VCSEL (a different

$$
\begin{aligned}
G_{Diff}(T_J) &= \frac{dg_{st}}{dN_e}(T_J) \\
&= \frac{\Gamma_{QW} N_{QW} g_{QW} \pi \hbar^2}{A_{QW} K_B T_J} \\
&\quad \times \{ \frac{\frac{\exp(\frac{E_{e,L}(T_J)-F_e}{k_B T_J})}{[\exp(\frac{E_{e,L}(T_J)-F_e}{k_B T_J})+1]^2}}{N_{QW} m_e [\frac{1}{\exp(-\frac{E_{C,Bulk}(T_J)-F_e}{k_B T_J})+1} - \frac{1}{\exp(-\frac{E_{e,1}(T_J)-Fe}{k_B T_J})+1}] + \left(N_{QW} L_{z,QW} m_e^{\frac{3}{2}} + L_{z,Bulk} m_{e,Bulk}^{\frac{3}{2}}\right) \left(\frac{k_B T_J}{2\pi\hbar^2}\right)^{\frac{1}{2}} \exp(\frac{E_{C,Bulk}(T_J)-F_e}{k_B T_J})} \\
&= \frac{\Gamma_{QW} N_{QW} g_{QW} \pi \hbar^2}{A_{QW} k_B T_J} \\
&\quad + \frac{\frac{\exp(\frac{E_{h,L}(T_J)-F_h}{k_B T_J})}{[\exp(\frac{E_{h,L}(T_J)-F_h}{k_B T_J})+1]^2}}{N_{QW} \sum_{m=1}^{2} m_{h,m} [\frac{1}{\exp(\frac{E_{V,Bulk}(T_J)-F_h}{k_B T_J})+1} - \frac{1}{\exp(\frac{E_{h,m}(T_J)-F_h}{k_B T_J})+1}] + \left(N_{QW} L_{z,QW} m_h^{\frac{3}{2}} + L_{z,Bulk} m_{h,Bulk}^{\frac{3}{2}}\right) \left(\frac{k_B T_J}{2\pi\hbar^2}\right)^{\frac{1}{2}} \exp(\frac{E_{V,Bulk}(T_J)-F_h}{k_B T_J})} \}
\end{aligned}
\tag{9}
$$

TABLE I

THRESHOLD CURRENT, MAXIMUM POWER, DIFFERENTIAL QUANTUM EFFICIENCY (DQE), POWER CONVERSION EFFICIENCY (PCE) AND VOLTAGE AT 10 kA/cm^2 FOR OXIDE-FREE VCSELs SIZE FROM 1 TO3 μm

Device Size (μm)	I_{th} (mA)	P_{max} (mW)	DQE	PCE	V at 10 kA/cm^2(V)
1	0.33	5.00	79.7%	37.4%	1.273
1.5	0.31	7.34	76.8%	42.0%	1.315
2	0.30	7.97	73.4%	45.5%	1.381
2.5	0.28	8.74	79.8%	47.2%	1.410
3	0.32	11.61	76.0%	49.0%	1.413

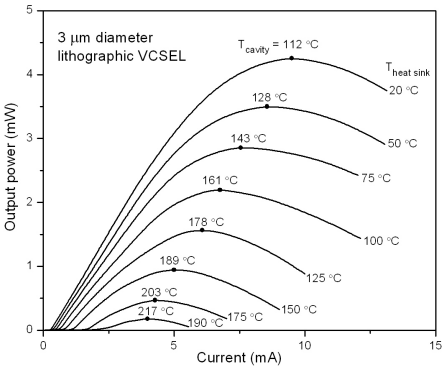

Fig. 6. Internal VCSEL temperature and spectral gain offset for a 3 μm diameter oxide-free VCSEL.

device design than used in Fig. 5 and Table I) that illustrates the internal temperature rise measured due to self-heating that causes thermal rollover. Electrical resistance is higher in the VCSEL of Fig. 6, and this causes an increase in self-heating.

The LI measurements are performed taken from 20 °C to 190 °C heat sink temperatures. The internal temperature is tracked using the known temperature shift of the lasing resonance with temperature. Spectral analysis is performed to identify the lowest order transverse mode of the cavity, and this mode is tracked for measurements at different mount temperatures and bias currents. For the device of Fig. 6, the 3 μm VCSEL becomes multimode at high bias current density. A constant value for wavelength shift was assumed to be 0.07 nm. Fig. 6 shows that at the heat sink temperature of 20 °C, the VCSEL reaches a thermal rollover at an internal device temperature of 112 °C at a bias current of $\sim$ 9 mA. While the VCSEL continues to produce stimulated emission and lasing for higher currents, its output power and therefore internal photon density have saturated and are decreasing with further increase in current.

Effects such as spatial hole burning have not been analyzed, but are important. These effects are beyond the current analysis and should be included in future works to both quantify and study their impact in more detail.

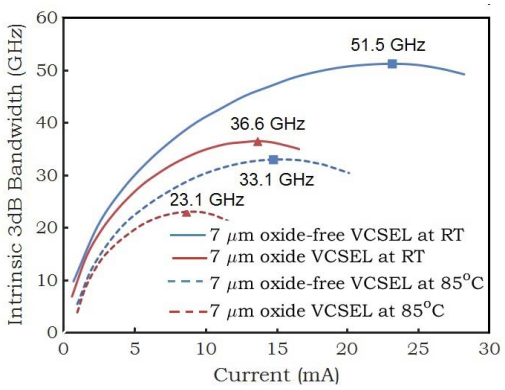

Fig. 7. Comparison of intrinsic modulation 3dB bandwidth on bias current for 7 μm oxide and oxide-free VCSELs at stage temperature of RT and 85°C. Red triangles and blue squares indicate the calculated maximum intrinsic modulation bandwidth for the oxide and oxide-free VCSELs, respectively.

IV. OXIDE VS. OXIDE-FREE V CSEL INTRINSIC MODULATION SPEED

The LIV curves produce both the output power from the lasers, while their cavity designs provide the value of the photon density within the cavity that produces the laser power. This photon density is extracted from the output power based on the cavity design and efficiency and compared with the calculated differential gain for either oxide or oxide-free VCSELs. The measured LIV and thermal resistance parameters can then be used to predict the intrinsic VCSEL speeds for both oxide and oxide-free cavities.

The measured results and analysis show that there are two ways that can be combined to increase the intrinsic modulation speed of the VCSEL given otherwise optimal cavity and gain designs. One way is to reduce the VCSEL's thermal resistance while maintaining efficiency and low electrical parasitics. The second way, which can be combined with reducing the thermal resistance, is to reduce the VCSEL cavity size. Both changes in device and cavity structure will reduce the internal operating temperature for a given set of bias conditions as long as high efficiency is maintained. When used together, reducing thermal resistance and scaling to smaller size while maintaining laser diode efficiency are predicted to provide the route to very high modulation speeds in future miniature VCSELs.

Figures 7 and 8 show results from the calculations that compare values for measured LIV's from either oxide or oxide-free VCSELs. The parameters of the 7 μm diameter oxide VCSEL are given in a publication by Chalmers University [20] and then are used to our intrinsic modulation model to calculate the differential gain, photon number and junction temperature at stage temperature of RT and 85 °C. The dependencies of calculated differential gain, photon number and junction temperature vs. bias current with different thermal resistance for either 7 μm oxide or oxide-free VCSELs are compared. The saturation of the output power due to self-heating causing spectral detuning, and this eventually saturates the intrinsic modulation speed. However, Fig. 7 still leaves open whether the saturation in speed is due to differential gain decrease or saturation of the photon density.

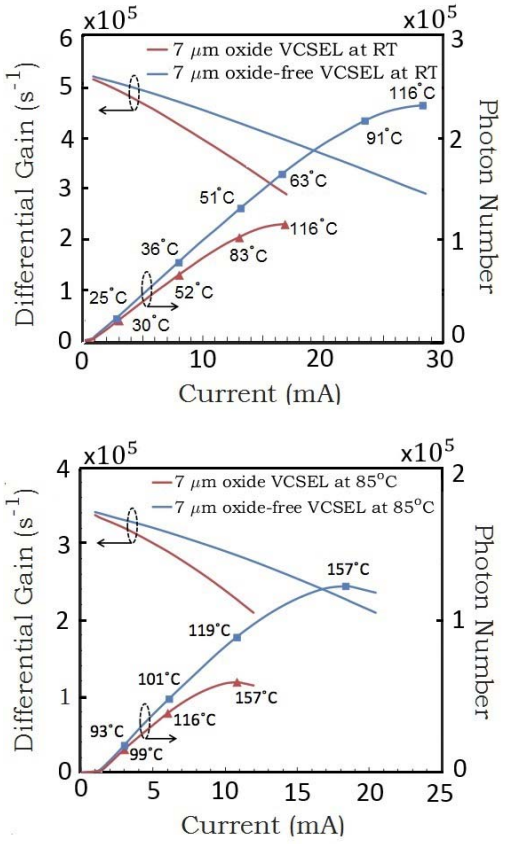

Fig. 8. Comparison of differential gain, photon number and junction temperature vs. bias current between 7 μm diameter oxide and oxide-free VCSELs. Upper: At stage temperature of RT. Lower: At stage temperature of 85°C.

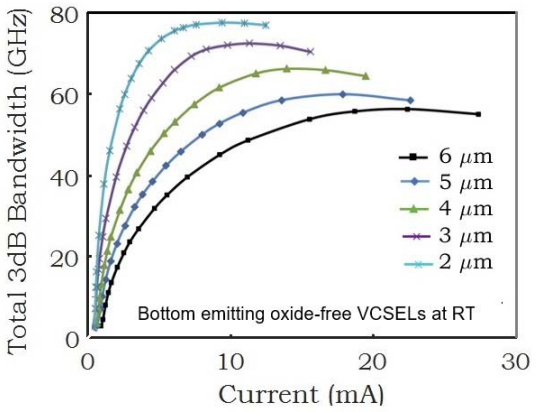

Fig. 9. Total modulation 3dB bandwidth calculations for bottom-emitting oxide-free VCSELs.

Fig. 7 shows that the lower thermal resistance of the oxide-free VCSEL combined with its high efficiency enables a higher bias current prior thermal rollover temperature and thereby a higher stimulated emission rate. The maximum intrinsic modulation bandwidth of the oxide-free VCSEL for both stage temperatures increases significantly by 40% over the oxide VCSEL.

Already even for rather large aperture sizes the results predict that small signal intrinsic bandwidth of > 50 GHz is possible at room temperature, suggesting that 100 Gb/s optical data speed could be possible. Below we show size scaling further strengthens this prediction.

Fig. 8 shows the dependence of the differential gain and photon density on bias current for room temperature (RT) and 85 °C operation. The differential gain decreases with increasing the bias current due to self-heating and spectral detuning for both operating temperatures, but still remains moderately high at the thermal rollover. In contrast it is the abrupt saturation in photon density that limits the stimulated emission rate as set by the combined photon density and the differential gain, with the differential gain estimate from Eq. (9).

In Fig. 8, the photon number is extracted from the L-I and the known cavity characteristics. The parameters of thermal resistance and efficiency are also given in the L-I-V characteristics [20]. This enables us to extract the contributions of differential gain and the photon number (photon density) for different drive levels. These are then used to determine the 3 dB intrinsic bandwidth of Fig. 7. The oxide-free VCSEL has improved performance at higher drive levels due to its better thermal properties. The internal temperature at roll over was found to be similar for the two VCSELs despite different designs. In general, the rollover can be controlled through improved active region designs.

The size dependence of the 3 dB bandwidth accounting for junction temperature of the oxide-free VCSEL has also been studied as it depends on current. This is shown in Fig. 9. As shown in Table I, the high efficiency and low thermal resistance that can be achieved with the oxide-free aperture results in high drive current density prior to thermal rollover of the output power. This high drive current density in turn produces high photon density. As the VCSEL size decreases, and as long as its efficiency can be maintained with low thermal resistance, the analysis predicts intrinsic speed can be increased by reducing the laser cavity size. As opposed to an optical effect however, the decrease is due to the reduced junction temperature that can be obtained for a given photon density in the cavity.

Fig. 9 shows the impact of size reduction to further reduce internal device temperature while producing a high photon density in the laser cavity. These calculations now assume device parameters, as opposed to taking these values from experimental L-I-Vs. The L-I-V's, including thermal rollover, are calculated an internal capacitance and electrical resistance based on epitaxial design. However, the analysis does not include lateral diffusion of electrons and holes that creates a lateral charge region outside the VCSEL aperture. This electron-hole density that exists in the ring just outside the perimeter of the oxide aperture can create significant capacitance. This capacitance can be reduced using a buried heterostructure. The analysis for Fig. 9 predicts an increasing intrinsic bandwidth for small cavity lasers along with a small signal room temperature small signal modulation bandwidth of almost 80 GHz for a 2 μm oxide-free VCSEL. This extremely high intrinsic speed can enable direct modulation

data rates $\geq$ 100 Gb/s. Moreover, the 2 μm cavity size produces single mode operation, so that the high speed optical data can be transmitted over single mode fiber. Even the 6 μm VCSEL size is projected to be capable of an intrinsic modulation speed of 50 GHz, although at a very high bias current. This also shows the importance of being able to size scale the VCSEL cavity with a controllable aperture. Size scaling is important to both maximize speed and minimize bit energy.

Further scaling is possible using oxide-free apertures, since transverse mode sizes as small as 100 nm diameter for 1 μm free space emission wavelength has been demonstrated [44]. Electrical parasitics will also play a critical role. These electrical parasitics have also been analyzed and will be presented elsewhere. What we find is that as the VCSEL is scaled in cavity size, it also becomes possible to scale electrical contacting and use additional internal confinement schemes in the oxide-free VCSEL to decrease the electrical parasitics. Our analysis is consistent with 100 Gb/s projection for direct modulation considering these electrical parasitics, and apparently unlimited by the intrinsic response. The oxide-free aperture enables greater flexibility in design to address these internal device parastics.

V. Summary

Advanced VCSEL technology is analyzed to determine its potential for future very high speed optical interconnects based on directly modulated lasers. The limitations in today's directly modulated VCSELs appear to come from self-heating during high temperature operation of 85°C. Oxide-free VCSELs that use oxide-free apertures have been compared with oxide VCSELs that use oxide apertures. Oxide-free apertures have been found to greatly reduce thermal resistance while maintaining high efficiency, even for small sized VCSELs. The improved thermal resistance and smaller laser size promise much higher directly modulated laser speed in the future technology.

The specific limitations of the temperature dependent differential gain and photon saturation were analyzed using a model that we believe is one of the first if not the first to include spectral detuning and thermal broadening in the analysis of self-heating. The two temperature dependent mechanisms of differential gain and photon density were studied to determine their limitations on modulation speed. While the differential gain is found to decrease with increasing bias current due to internal self-heating, it does not limit the VCSEL's intrinsic speed. This is because it has a relative small decrease with temperature over the full range of operation prior to saturation of the cavity photon density. Instead, the abrupt saturation of the cavity photon density is found responsible for limiting the laser's intrinsic speed.

Oxide VCSELs represent the highest speed directly modulated laser diodes available today commercially or in the laboratory. In the laboratory, direct modulation data rates in excess of 60 Gb/s have been demonstrated. Oxide VCSELs followed proton implanted VCSELs, and brought advantages because their cavity sizes could be scaled and yet produce high efficiency lasing. The next generation VCSEL technologies promise to be higher speed and even more efficient through size scaling and new aperture designs, such as the oxide-free aperture.

References

[1] H. Soda, K.-C. Iga, C. Kitahara, and Y. Suematsu, "GaInAsP/InP surface emitting injection lasers," *Jpn. J. Appl. Phys.*, vol. 18, no. 12, pp. 2329–2330, Dec. 1979.

[2] F. Koyama, S. Kinoshita, and K. Iga, "Room-temperature continuous wave lasing characteristics of a GaAs vertical cavity surface-emitting laser," *Appl. Phys. Lett.*, vol. 55, no. 3, pp. 221–222, 1989.

[3] J. P. Van der Ziel and M. Ilegems, "Multilayer GaAs-$Al_{0.3}Ga_{0.7}$as dielectric quarter wave stacks grown by molecular beam epitaxy," *Appl. Opt.*, vol. 14, no. 11, pp. 2627–2630, 1975.

[4] M. Ogura, T. Hata, N. J. Kawai, and T. Yao, "GaAs/Al_xGa_{1-x} as multilayer reflector for surface emitting laser diode," *Jpn J. Appl. Phys.*, vol. 22, no. 2A, pp. L112–L114, 1983.

[5] P. L. Gourley, "Single crystal semiconductor multilayers for electrically active optical interference filters," *Superlattices Microstruct.*, vol. 1, no. 3, pp. 227–230, 1985.

[6] P. L. Gourley and T. J. Drummond, "Single crystal, epitaxial multilayers of AlAs, GaAs, and Al_XGa_{1-x}as for use as optical interferometric elements," *Appl. Phys. Lett.*, vol. 49, no. 9, pp. 489–491, 1986.

[7] P. L. Gourley and T. J. Drummond, "Visible, room-temperature, surface-emitting laser using an epitaxial Fabry–Pérot resonator with AlGaAs/AlAs quarter-wave high reflectors and AlGaAs/GaAs multiple quantum wells," *Appl. Phys. Lett.*, vol. 50, no. 18, pp. 1225–1227, 1987.

[8] J. L. Jewell *et al.*, "Vertical cavity single quantum well laser," *Appl. Phys. Lett.*, vol. 55, no. 5, pp. 424–426, 1989.

[9] A. Ibaraki, K. Kawashima, K. Furusawa, T. Ishikawa, T. Yamaguchi, and T. Niina, "Buried heterostructure GaAs/GaAlAs distributed Bragg reflector surface emitting laser with very low threshold (5.2 mA) under room temperature CW conditions," *Jpn. J. Appl. Phys.*, vol. 28, no. 4, pp. L667–L668, 1989.

[10] K. Tai *et al.*, "Room-temperature continuous-wave vertical-cavity surface-emitting GaAs injection lasers," *Appl. Phys. Lett.*, vol. 55, no. 24, pp. 2473–2475, 1989.

[11] K. Tai, R. J. Fischer, K. W. Wang, S. N. G. Chu, and A. Y. Cho, "Use of implant isolation for fabrication of vertical cavity surface-emitting laser diodes," *Electron. Lett.*, vol. 25, no. 24, pp. 1644–1645, Nov. 1989.

[12] K. Tai, L. Yang, Y. H. Wang, J. D. Wynn, and A. Y. Cho, "Drastic reduction of series resistance in doped semiconductor distributed Bragg reflectors for surface-emitting lasers," *Appl. Phys. Lett.*, vol. 56, no. 25, pp. 2496–2498, 1990.

[13] Y. H. Lee, J. L. Jewell, A. Scherer, S. L. McCall, J. P. Harbison, and L. T. Florez, "Room-temperature continuous-wave vertical-cavity single-quantum-well microlaser diodes," *Electron. Lett.*, vol. 25, no. 20, pp. 1377–1378, Sep. 1989.

[14] T. Yoshie *et al.*, "Vacuum Rabi splitting with a single quantum dot in a photonic crystal nanocavity," *Nature*, vol. 432, no. 7014, pp. 200–203, Nov. 2004.

[15] D. M. Kuchta *et al.*, "A 50 Gb/s NRZ modulated 850 nm VCSEL transmitter operating error free to 90 °C," *J. Lightw. Technol.*, vol. 33, no. 4, pp. 802–810, Feb. 15, 2015.

[16] D. M. Kuchta *et al.*, "A 71-Gb/s NRZ modulated 850-nm VCSEL-based optical link," *IEEE Photon. Technol. Lett.*, vol. 27, no. 6, pp. 577–580, Mar. 15, 2015.

[17] F. Tan, M.-K. Wu, M. Liu, M. Feng, and N. Holonyak, "850 nm oxide-VCSEL with low relative intensity noise and 40 Gb/s error free data transmission," *IEEE Photon. Technol. Lett.*, vol. 26, no. 3, pp. 289–292, Feb. 1, 2014.

[18] N. Iwai *et al.*, "1060 nm VCSEL array for optical interconnection," *Furukawa Rev.*, vol. 36, pp. 1–4, Mar. 2009.

[19] E. Haglund *et al.*, "30 GHz bandwidth 850 nm VCSEL with sub-100 fJ/bit energy dissipation at 25–50 Gbit/s," *Electron. Lett.*, vol. 51, no. 14, pp. 1096–1098, Jul. 2015.

[20] P. Westbergh *et al.*, "High-speed oxide confined 850-nm VCSELs operating error-free at 40 Gb/s up to 85 °C," *IEEE Photon. Technol. Lett.*, vol. 25, no. 8, pp. 768–771, Apr. 15, 2013.

[21] A. Larsson, P. Westbergh, J. Gustavsson, and Å. Haglund, "High-speed low-current-density 850 nm VCSELs," *Proc. SPIE*, vol. 7615, p. 761505, Feb. 2010.

[22] C. Y. Wang, M. Liu, M. Feng, and N. Holonyak, "Temperature dependent analysis of 50 Gb/s oxide-confined VCSELs," in *Proc. Opt. Fiber Commun. Conf. Exhib.*, Mar. 2017, pp. 1–3.

[23] C. Y. Wang, M. Liu, M. Feng, and N. Holonyak, Jr., "Microwave extraction method of radiative recombination and photon lifetimes up to 85 °C on 50 Gb/s oxide-vertical cavity surface emitting laser," *J. Appl. Phys.*, vol. 120, no. 22, p. 223103, 2016.

[24] P. Westbergh, J. S. Gustavsson, Â. Haglund, M. Skold, A. Joel, and A. Larsson, "High-speed, low-current-density 850 nm VCSELs," *IEEE J. Sel. Top. Quantum Electron.*, vol. 15, no. 3, pp. 694–703, Mar./Jun. 2009.

[25] T. Yoshie, J. Vučković, A. Scherer, H. Chen, and D. Deppe, "High quality two-dimensional photonic crystal slab cavities," *Appl. Phys. Lett.*, vol. 79, pp. 4289–4291, Dec. 2001.

[26] T. Yoshie, A. Scherer, H. Chen, D. L. Huffaker, and D. Deppe, "Optical characterization of two-dimensional photonic crystal cavities with indium arsenide quantum dot emitters," *Appl. Phys. Lett.*, vol. 79, pp. 114–116, Jul. 2001.

[27] T. Yang, O. Shchekin, J. D. O'Brien, and D. G. Deppe, "Room temperature, continuous-wave lasing near 1300 nm in microdisks with quantum dot active regions," *Electron. Lett.*, vol. 39, no. 13, pp. 1657–1658, Nov. 2003.

[28] D. G. Deppe, L. Mingxin, and X. Yang, "Metal cavities as the efficiency killer in nanolasers and spontaneous light sources," presented at the CLEO, San Jose, CA, USA, Jun. 2013.

[29] M. A. Zimmler, F. Capasso, S. Müller, and C. Ronning, "Optically pumped nanowire lasers: Invited review," *Semicond. Sci. Technol.*, vol. 25, Jan. 2010, Art. no. 024001.

[30] F. Koblmüller, B. Mayer, T. Stettner, G. Abstreiter, and J. J. Finley, "GaAs–AlGaAs core–shell nanowire lasers on silicon: Invited review," *Semicond. Sci. Technol.*, vol. 32, Apr. 2017, Art. no. 053001.

[31] Z. Huang, C. C. Lin, and D. G. Deppe, "Spontaneous lifetime and quantum efficiency in light emitting diodes affected by a close metal mirror," *IEEE J. Quant. Electron.*, vol. 29, no. 12, pp. 2940–2949, Dec. 1993.

[32] H. Kuhn, "Classical aspects of energy transfer in molecular systems," *J. Chem. Phys.*, vol. 53, pp. 101–108, Jul. 1970.

[33] D. L. Huffaker, D. G. Deppe, K. Kumar, and T. J. Rogers, "Native-oxide defined ring contact for low threshold vertical-cavity lasers," *Appl. Phys. Lett.*, vol. 65, no. 1, pp. 97–99, Jun. 1994.

[34] G. M. Yang, M. H. MacDougal, and P. D. Dapkus, "Ultralow threshold current vertical-cavity surface-emitting lasers obtained with selective oxidation," *Electron. Lett.*, vol. 31, no. 11, pp. 886–888, May 1995.

[35] D. L. Huffaker and D. G. Deppe, "Intracavity contacts for low-threshold oxide-confined vertical-cavity surface-emitting lasers," *IEEE Photon. Technol. Lett.*, vol. 11, no. 8, pp. 934–936, Aug. 1999.

[36] R. Jager *et al.*, "57% wallplug efficiency oxide-confined 850 nm wavelength GaAs VCSELs," *Electron. Lett.*, vol. 33, no. 4, pp. 330–331, Feb. 1997.

[37] X. Yang, M. Li, G. Zhao, Y. Zhang, S. Freisem, and D. Deppe, "Small-sized lithographic single-mode VCSELs with high-power conversion efficiency," *Proc. SPIE*, vol. 9381, pp. 93810R-1–93810R-6, Mar. 2015.

[38] J. M. Dallesasse, N. Holonyak, Jr., A. R. Sugg, T. A. Richard, and N. El-Zein, "Hydrolyzation oxidation of Al_xGa_{1-x} As-AlAs-GaAs quantum well heterostructures and superlattices," *Appl. Phys. Lett.*, vol. 57, pp. 2844–2846, Oct. 1990.

[39] J. M. Dallesasse and D. G. Deppe, "III–V oxidation: Discoveries and applications in vertical-cavity surface-emitting lasers," *Proc. IEEE*, vol. 101, no. 10, pp. 2234–2242, Oct. 2013.

[40] G. Zhao *et al.*, "Record low thermal resistance of mode-confined VCSELs using AlAs/AlGaAs DBRs," presented at the CLEO, San Jose, CA, USA, Jun. 2013, pp. 1–2.

[41] X. Yang, G. Zhao, M. Li, and D. Deppe, "Stress test of lithographic vertical-cavity surface-emitting lasers under extreme operating conditions," *Electron. Lett.*, vol. 51, no. 16, pp. 1279–1280, Aug. 2015.

[42] X. Yang, M. Li, G. Zhao, S. Freisem, and D. G. Deppe, "Small oxide-free vertical-cavity surface-emitting lasers with high efficiency and high power," *Electron. Lett.*, vol. 50, no. 24, pp. 1864–1866, Nov. 2014.

[43] X. Yang, M. Li, G. Zhao, Y. Zhang, S. Freisem, and D. G. Deppe, "Oxide-free vertical-cavity surface-emitting lasers with low junction temperature and high drive level," *Electron. Lett.*, vol. 50, no. 20, pp. 1474–1475, Sep. 2014.

[44] A. Müller *et al.*, "Self-aligned all-epitaxial microcavity for cavity QED with quantum dots," *Nano Lett.*, vol. 6, pp. 2920–2924, Nov. 2006.

Dennis G. Deppe (F'00) received the B.S., M.S., and Ph.D. degrees from the University of Illinois at Urbana–Champaign, Urbana, in 1981, 1985, and 1988, all in electrical engineering. His Ph.D. thesis centered on atom diffusion in III–V semiconductor heterostructures and its use in superlattice disordering and laser fabrication.

He was a Member of Technical Staff with AT&T Bell Laboratories, Murray Hill, NJ, USA, where he researched and developed vertical-cavity surface-emitting lasers. In 1990, he joined The University of Texas at Austin, where he became a Professor with the Electrical and Computer Engineering Department and held the Cullen Trust Endowed Professorship in engineering. He currently holds the Florida Photonics Center of Excellence Endowed Chair in nanophotonics at the University of Central Florida, Orlando. His recent research interests include optoelectronics, laser physics, epitaxial crystal growth, and quantum optics. His research has included a number of firsts, including the identification of the Si-vacancy complex as responsible for Si diffusion in GaAs and AlGaAs, the identification of the p-dopant base diffusion mechanism in III–V bipolar transistors, the first demonstration of a continuous-wave laser on Si, the first oxide-confined VCSEL, the first GaAs-based 1.3-μm quantum-dot laser diode, and the first demonstrations of high T_0 quantum-dot laser diodes.

He has authored or coauthored over 200 journal articles and presented over 200 conference papers in the area of III–V semiconductors.

Dr. Deppe has received the Nicholas Holonyak Jr. Award from the Optical Society of America and the IEEE LEOS Engineering Achievement Award, and served as an IEEE LEOS Distinguished Lecturer. He is a fellow of the OSA.

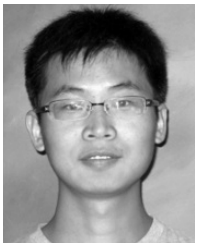

Mingxin Li received the B.S. degree in optical engineering from Zhejiang University, China, in 2010, the M.S. degree in optics from the College of Optics and Photonics, University of Central Florida, Orlando, FL, USA, in 2011, and the Ph.D. degree in optics from the College of Optics and Photonics, University of Central Florida, Orlando, USA, in 2016.

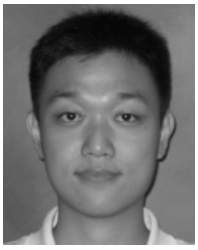

Xu Yang received the B.S. degree in physics from the Department of Physics, Tsinghua University, China, in 2008, and the M.S. degree in optical engineering from the Department of Precision Instruments, Tsinghua University, in 2010, and the Ph.D. degree in optics from the College of Optics and Photonics, University of Central Florida, Orlando, USA, in 2016. He is currently a Research and Development Engineer in semiconductor lasers with Accelink Company, Wuhan, Hubei, China.

Mina Bayat was born in Zanjan, Iran. She received the B.S. degree *(magna cum laude)* in electrical engineering from the University of Tabriz, Tabriz, Iran, in 2007, and the M.S. degree in electrical engineering from the Sharif University of Technology, Tehran, Iran, in 2010, and the M.Sc. degree in optics from the College of Optics and Photonics, University of Central Florida, Orlando, USA, in 2015, where she is currently pursuing the Ph.D. degree in optics. Her current research interests include fabrication, design, and simulations of VCSELs and semiconductor lasers.